ARTICLE

Effect of Protein Dimerization on Ion Conductivity of Gramicidin A Channel Studied Using Polarizable Force Field

Jun-ben Weng[a,b†], Chen-yi Liao[a†], Yan Li[a], Ding-lin Zhang[a], Guo-hui Li[a*], An-hui Wang[a,c*]

a. Laboratory of Molecular Modeling and Design, State Key Laboratory of Molecular Reaction Dynamics, Dalian Institute of Chemical Physics, Chinese Academy of Sciences, Dalian 116023, China
b. University of Chinese Academy of Sciences, Beijing 101408, China
c. State Key Laboratory of Fine Chemicals, School of Chemistry, Dalian University of Technology, Dalian 116024, China

(Dated: Received on March 15, 2021; Accepted on April 6, 2021)

In studies of ion channel systems, due to the huge computational cost of polarizable force fields, classical force fields remain the most widely used for a long time. In this work, we used the AMOEBA polarizable atomic multipole force field in enhanced sampling simulations of single-channel gramicidin A (gA) and double-channel gA systems and investigated its reliability in characterizing ion-transport properties of the gA ion channel under dimerization. The influence of gA dimerization on the permeation of potassium and sodium ions through the channel was described in terms of conductance, diffusion coefficient, and free energy profile. Results from the polarizable force field simulations show that the conductance of potassium and sodium ions passing through the single- and double-channel agrees well with experimental values. Further data analysis reveals that the molecular mechanism of protein dimerization affects the ion-transport properties of gA channels, *i.e.*, protein dimerization accelerates the permeation of potassium and sodium ions passing through the double-channel by adjusting the environment around gA protein (the distribution of phospholipid head groups, ions outside the channel, and bulk water), rather than directly adjusting the conformation of gA protein.

Key words: Dimerization, Conductance, Gramicidin A, AMOEBA force field, Umbrella sampling

I. INTRODUCTION

In living organisms, the transport of ions through pores in membranes plays a key role in a series of life processes such as intercellular communication, signal transduction, osmotic stress response, and muscle contraction. Ion channels are widespread membrane proteins that allow specific kinds of ions to pass through the channel under an electrochemical gradient, thereby regulating the potential difference between two sides of the cell membrane [1–3]. The imbalance of ion channels can cause a range of diseases such as muscle paralysis and epilepsy, so ion channels are also extremely important drug targets.

The cell membrane is a crowded environment. For example, 25% of the area of the red blood cell membrane is occupied by proteins, and the proportion can reach 40% in the bacterial outer membrane [4–6]. Many membrane proteins are not uniformly distributed in the cell membrane, and the aggregation of membrane proteins, especially ion channels in the cell membrane, constitutes an important strategy for organisms to regulate signal transduction [7–11]. For example, Weingarth *et al.* employed solid-state NMR technology to identify that KcsA potassium ion channels in the open state could aggregate in the cell membrane, and the aggregated KcsA shows a higher ion-transport efficiency [11]. Further coarse-grained molecular dynamics (MD) simulations revealed that the M0 helix near the N-terminus

†These authors contributed equally to this work.
*Authors to whom correspondence should be addressed. E-mail: ghli@dicp.ac.cn, wangah@dicp.ac.cn

of the KcsA channel could simultaneously control opening/closing and aggregation of the channel.

Gramicidin A (gA) studied here is one of the simplest ion channels. It is consisted of two monomers connected head-to-head by hydrogen bonds, and each monomer contains only 15 residues. Available data from experiments [12–15] and simulations [16] both show that gA can aggregate to form double-channel in phospholipid membranes.

With the development of computer technology, molecular dynamics (MD) simulations are becoming increasingly important in studies of biological systems [17–20]. In MD simulation studies of ion channel properties, due to the huge computational cost of polarizable force fields, classical force fields remain the most widely used for a long time. For classical force fields like AMBER [21] and CHARMM [22], the atomic charge is fixed during the simulation since the charge redistribution caused by local environmental changes is not well considered. However, when the ion passes through the channel, the local environment of the ion changes greatly, and the movement of the ion also causes the surrounding environment to change, making it difficult for the classical force fields to accurately describe the ion permeation process. For example, experimental data [23, 24] show that the free energy barrier for a potassium ion passing through the gA channel should be less than 10 kcal/mol, while most simulation data [25–28] with classical force field yield a free energy barrier more than 10 kcal/mol. Furthermore, the channel conductance calculated from simulations with a classical force field is three orders of magnitude lower than that from experiments [25, 26, 29].

Recently, we have developed AMOEBA polarizable force field parameters for different types of phospholipid molecules [30] and calculated the free energy changes of K^+ and Na^+ passing through the gA channel using the AMOEBA force field. The results were in good agreement with experimental values, showing high reliability of polarizable force field in ion channel simulations [31]. In this work, enhanced sampling simulations of single-channel and double-channel gA systems with AMOEBA polarizable force field were performed to investigate the differences in free energy and conductance of K^+ and Na^+ passing through single- and double-channels. Moreover, the molecular mechanism of dimerization affecting the channel function was revealed by employing free energy decomposition and coordination atom analysis.

II. MATERIALS AND METHODS

A. Simulation systems

The initial structure of single-channel gA was derived from the NMR structure in the Protein Data Bank (PDB ID 1JNO). The protein-membrane-solution system was constructed via the CHARMM-GUI (http://www.charmm-gui.org/) server from which the single-channel gA was embedded in a phospholipid bilayer composed of 96 dimyristoyl-sn-glycero-3-phosphocholine (DMPC). The DMPC bilayer was then filled with the solvent of 15 Å thickness on each side and 1.0 mol/L NaCl was added to neutralize the net charge of the system. The single-channel gA system was equilibrated in 10 ns NPT simulation, and the last frame of the trajectory was used as the initial structure for subsequent umbrella sampling simulations (FIG. 1(a)).

The structure of the double-channel gA was obtained by molecular docking of two single-channel gAs. Three representative structures with the highest ZDOCK [32] docking scores were embedded in a phospholipid bilayer consisting of 96 DMPC by CHARMM-GUI, respectively. Each DMPC bilayer was then filled with the solvent of 15 Å thickness on each side and 1.0 mol/L NaCl was added to neutralize the net charge of the system. To obtain a more reasonable double-channel structure, eight independent equilibrium NPT simulations of 300 ns were carried out for each representative system. Then, the trajectories were collected and clustered based on protein backbone atoms, and the cluster center with the highest population was used as the initial structure for subsequent double-channel system umbrella sampling simulations (FIG. 1(b)).

All simulations for equilibrium stage processes were carried out in OpenMM [33]. The AMOEBA force field parameters for K^+, Na^+, Cl^- and water were taken from the amoebapro13.prm file of the TINKER [34] package. The parameters for D-amino acids in gA were obtained from corresponding L-amino acids while the parameters for the formyl, ethanolamide groups, and DMPC were obtained from our previous work [31]. For simulation setup, the cutoff of the non-bonded interactions was 10 Å, and the PME [35] algorithm was used for electrostatic interactions. The time step was set to 2 fs. The temperature was maintained at 330 K using Andersen thermostat, and the pressure was kept at 1.0 bar using Monte Carlo anisotropic barostat. Mu-

DOI:10.1063/1674-0068/cjcp2103046

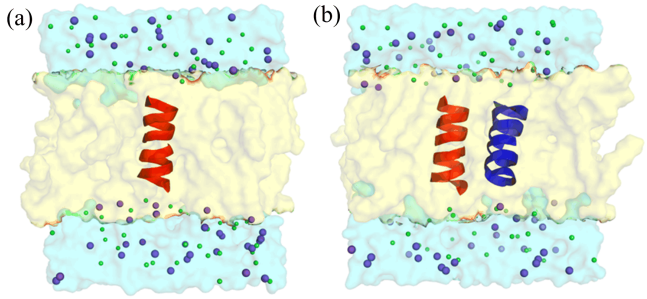

FIG. 1 Simulation systems for (a) single- and (b) double-channel of gA.

tual polarization was used, which employed the self-consistent field (SCF) with the Direct Inversion in Iterative Subspace (DIIS) method [36] to calculate the induced dipole moment. The convergence threshold of the induced dipole moment in SCF iteration was set to 0.0005 D.

B. Umbrella sampling

In this work, umbrella sampling [37] was employed for enhanced sampling MD simulations of ions passing through the gA channels, and for double-channel system, one of the two gA channels was chosen. The ion position away from the center of the channel in the z direction was set as the reaction coordinate, and a harmonic potential was applied to restrain the movement of the ion in specified coordinate ranges. To ensure sufficient sampling of the ion passing through the channel, a 7 ns umbrella sampling simulation was conducted for each window, and the last 6 ns trajectories were collected for subsequent analysis. All umbrella sampling simulations were carried out in OpenMM, with the Plumed [38] package to apply harmonic potentials and monitor the change in reaction coordinates.

For K^+, 72 sampling windows in 0.5 Å interval were set to cover the reaction coordinate from −18 Å to 18 Å (z=0 at the center of the channel). The restraint with a force constant of 10 kcal·mol^{-1}Å^{-2} was applied to restrain movements of the K^+ in each window. For Na^+, 73 sampling windows in 0.3 Å interval with force constant of 15 kcal·mol^{-1}·Å^{-2} were set to cover the reaction coordinate region from −11 Å to 11 Å, while the region from −18 Å to −11 Å and 11 Å to 18 Å were sampled by 28 windows in 0.5 Å interval with force constant of 10 kcal·mol^{-1}·Å^{-2}. In addition to the z-direction restraint, a flat-bottom potential with force constant of 5 kcal·mol^{-1}·Å^{-2} was also applied to limit the ion motion in the XY-plane to within 5 Å of the channel centerline.

C. Trajectory analyses

1. Free energy calculation and decomposition

After the completion of umbrella sampling simulations, the free energy profile of ions passing through the channel could be reconstructed using the g_wham [39] module of the GROMACS [40] package. The free energy profile is asymmetric due to the simulation artifacts caused by the finite size of periodic systems [25, 29], the slow motion of phospholipid molecules [41, 42], and gA tilting [43–45] during MD simulations. To address this issue, the free energy profile was symmetrized using the method previously reported [29], and the free energy at z=±18 Å was used as the reference point by setting its free energy to 0.

Since the free energy change is equivalent to the thermodynamic reversible work in this process, the total free energy change can be decomposed into the contributions of different components [23]:

$$W_\alpha(z) - W_\alpha(z_0) = -\sum_\alpha \int_{z_0}^{z} \mathrm{d}z' \langle F_\alpha(z') \rangle \tag{1}$$

In this work, the free energy change was decomposed into the contributions of DMPC+bulk ions, bulk water, single-file water in the channel, and the gA channel itself (and the second gA channel).

2. Ion coordination number

The radial distribution function (RDF) was calculated using the g_rdf module in GROMACS, and the coordination number n_c of K^+ or Na^+ could be obtained by integrating the RDF $g(r)$:

$$n_c = 4\pi\rho \int_0^R r^2 g(r) \mathrm{d}r \tag{2}$$

where ρ is the concentration of oxygen atoms, and R is the position of the first minimum point for the RDF of ion-oxygen in bulk (K^+ is 3.6 Å, and Na^+ is 3.2 Å) [31].

3. Diffusion coefficient and maximum conductance

According to the one-dimensional Nernst-Plank equation, the diffusion coefficients of ions at different positions in the channel are required for the calculation of

DOI:10.1063/1674-0068/cjcp2103046

channel conductance. Here the GLE-HO [25, 46, 47] (Generalized Langevin Equation for a Harmonic Oscillator) method was used to calculate the ion diffusion coefficient. In the GLE-HO method, the diffusion coefficient $D(z_i)$ of the ion in the sampling window z_i could be expressed as a function of the normalized velocity autocorrelation function $C(t,\ z_i)$ of the ion motion in this umbrella sampling window:

$$D\left(z_i\right)=\lim_{s\to 0}\frac{-\hat{C}\left(s,z_i\right)\left\langle\delta z^2\right\rangle_i\left\langle\dot{z}^2\right\rangle_i}{\hat{C}\left(s,z_i\right)\left[s\langle\delta z^2\rangle_i+\langle\dot{z}^2\rangle_i/s\right]-\langle\delta z^2\rangle_i\langle\dot{z}^2\rangle_i} \quad (3)$$

where $\hat{C}(s, z_i)$ is the Laplace transformation of $C(t,\ z_i)$:

$$\hat{C}\left(s,z_i\right)=\int_0^\infty \mathrm{d}t\mathrm{e}^{-st}C\left(t,z_i\right) \quad (4)$$

Based on the one-dimensional Nernst-Plank equation and small-field approximation, the maximum conductance of the gA channel can be calculated by the following equation [25, 48–50]:

$$g_{\max}=\frac{e^2}{k_{\mathrm{B}}TL^2}\left\langle D(z)^{-1}\exp\left(\frac{+W(z)}{k_{\mathrm{B}}T}\right)\right\rangle^{-1}\cdot\left\langle\exp\left(\frac{-W(z)}{k_{\mathrm{B}}T}\right)\right\rangle^{-1} \quad (5)$$

where L is the effective length of the gA channel (28 Å), and e is the charge quantity of K^+ or Na^+.

III. RESULTS AND DISCUSSION

A. Free energy profiles during the K^+/Na^+ permeation

To ensure the convergence of free energy calculations, the cumulative umbrella sampling simulation time for K^+ or Na^+ reaches 500 ns or 700 ns for both single- and double-channel systems, respectively. The free energy profiles of ions passing through the gA channels are shown in FIG. 2. The free energy barrier obtained from simulations based on the AMOEBA force field is much lower than that based on the classical force field CHARMM27 [25, 26] and is closer to the experimentally determined free energy range [23, 24]. This result shows that the polarizable force field, which explicitly considers the polarization effect, can characterize the ion permeation process more accurately than classical force fields.

As shown in FIG. 2, for both single- and double-channel systems, the free energy barrier (relative to the binding site at the channel entrance) of K^+ passing through the channel is lower than that of Na^+, showing good agreement with the ion selectivity of the gA channel [23]. There are several local minima in the free energy profiles of both K^+ and Na^+, which correspond to different ion binding sites in the gA channel. For both single- and double-channel systems, the positions of these binding sites are the same, whereas the free energies of corresponding binding sites in double-channel are higher than those in the single-channel system, indicating that the binding affinity of ions to double-channel gA is weaker than that to single-channel gA. The difference is more striking for Na^+. As shown in FIG. 2(b), the free energy barrier of Na^+ passing through the double-channel gA (5.77 kcal/mol) is significantly lower

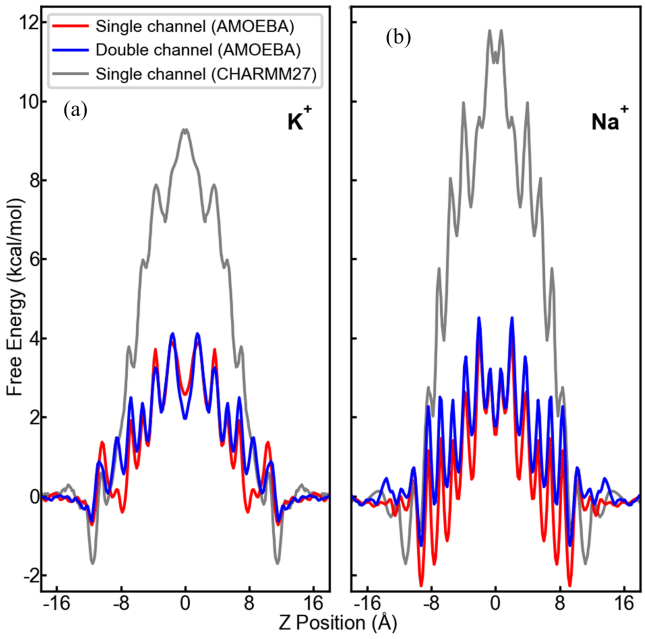

FIG. 2 Free energy profile of (a) K^+ and (b) Na^+ when ion passing through single- and double-channels. The free energies from the CHARMM27 force field were taken from Refs.[25, 26].

DOI:10.1063/1674-0068/cjcp2103046

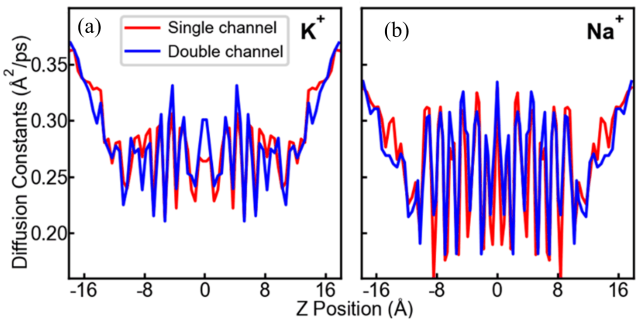

FIG. 3 Diffusion coefficients of (a) K^+ and (b) Na^+.

than that of the single-channel (6.24 kcal/mol), suggesting that gA dimerization actually affects the ion permeation process.

B. Comparison for conductance of gA channels

Calculations of the diffusion coefficients of K^+/Na^+ at different locations in the channel can further reveal the differences in the process of ions passing through single- and double-channel gAs. As shown in FIG. 3, the diffusion coefficients of ions in the channel are significantly smaller than those outside the channel, and there are several extreme points for the diffusion coefficients of both K^+ and Na^+. The location of these extreme points is consistent with the distribution of the extreme points of the free energy shown in FIG. 2. In line with the free energy profiles, the diffusion coefficients of Na^+ at all local minima are smaller than those of K^+, which further shows that K^+ is easier to pass through the gA channel. For single- and double-channel systems, there is essentially no difference in the location of these extremal points. However, for both ions, especially for Na^+, the diffusion coefficients at most minima of the double-channel system are slightly higher than those in the single-channel system, indicating that the diffusion rate of ions passing through consecutive binding sites in the double-channel is faster than that in the single-channel.

The maximum conductance of ions passing through the gA channel could be estimated using the GLE-HO equation with the diffusion coefficients and free energy profiles. As shown in Table I, the calculated conductance of Na^+ passing through the single-channel gA is much lower than that of K^+, and the conductance of both ions is very close to relevant experimental values, respectively, indicating that the conductance obtained from the AMOEBA force field is more reliable

TABLE I Conductance when ion passes through single- and double- gA channels.

Ion	Single channel		Double channel
	Expt.	Simu.	Simu.
K^+	23.8 [14], 26.0 [26]	29.5	36.9
Na^+	12.4 [14], 14.8 [26]	15.5	24.2

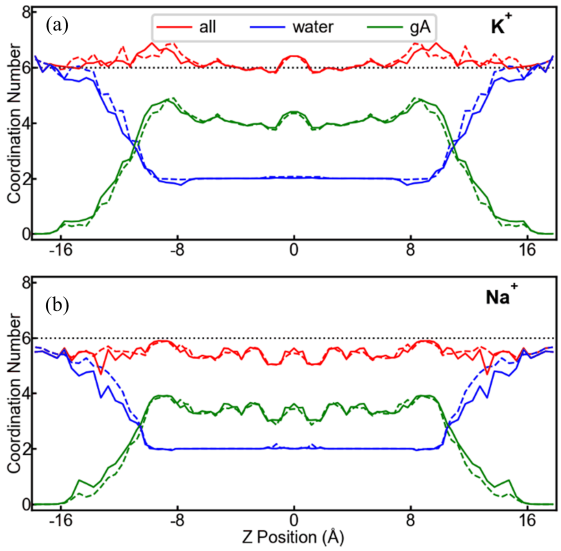

FIG. 4 Coordination numbers of (a) K^+ and (b) Na^+ with oxygen atoms when ion passing through single- and double-gA channels. The dashed and solid lines refer to the coordination numbers in single- and double-channel systems, respectively.

than those from classical force fields [25, 26, 29]. When passing through the double-channel, K^+ and Na^+ both exhibit higher conductance than in single-channel. This result is consistent with the previous report [13], reflecting the reliability of the AMOEBA force field to accurately describe the ion-transport properties of single- and double-channel gAs.

C. Rearrangements of coordination atoms during the K^+/Na^+ permeation

In the solution environment, ions can form coordination interactions with oxygen atoms of bulk water. Upon entering the narrow gA channel, the dehydration determines the selectivity of the channel for different ions. To describe the changes of coordination atoms when the ion passes through the channel, we further calculated the coordination number of the ion with oxygen atoms and the distribution of distances between the ion and carbonyl oxygen atoms at different positions in the channel.

DOI:10.1063/1674-0068/cjcp2103046

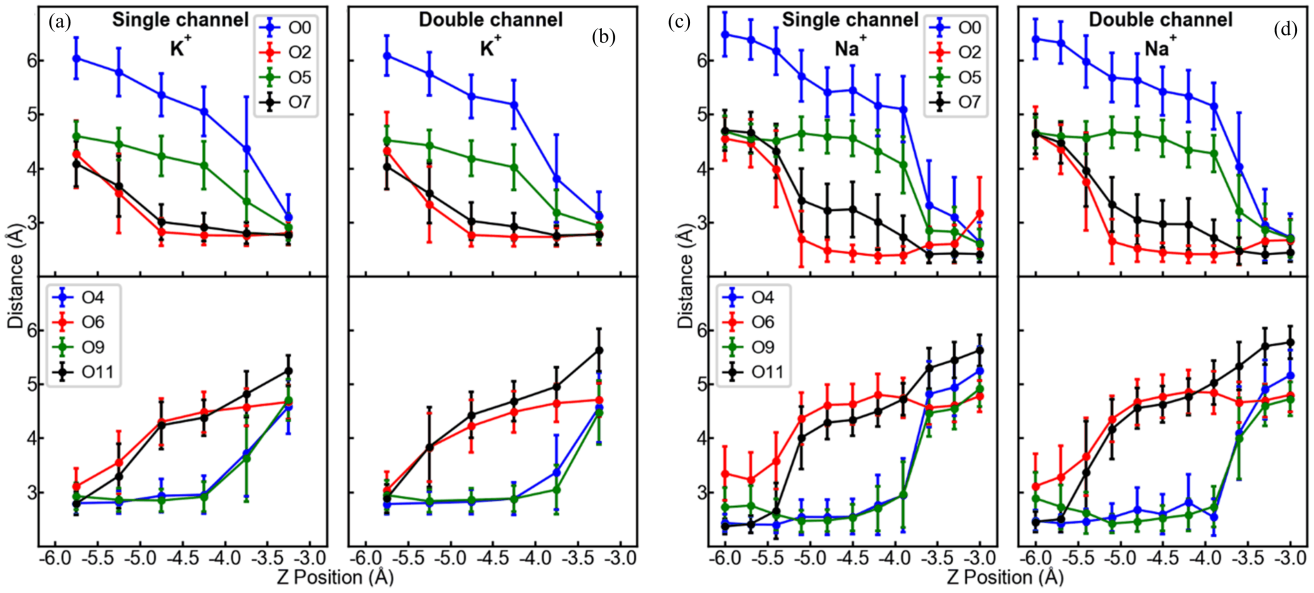

FIG. 5 Distances between K^+ (a, b) or Na^+ (c, d) with coordinating carbonyl oxygen atoms when ion passing through single- and double- gA channels. O0 refers to the oxygen atom on the formyl group of gA. O2, O4, O5, O6, O7, O9, and O11 refer to the carbonyl oxygen of Gly2, D-Leu4, Ala5, D-Val6, Val7, Trp9, and Trp11 of gA, respectively.

The total coordination number and the coordination number from water oxygen atoms or carbonyl oxygen atoms of gA protein are shown in FIG. 4. During the permeation of the ion, the total number of coordinated oxygen atoms remains essentially constant (6.2 for K^+ and 5.5 for Na^+). Before entering the channel ($|z|>$ 16 Å), the ion can form coordination with the oxygen atoms of water outside the channel; in the process of entering the channel (9 Å$<|z|<$16 Å), the water outside the channel that coordinates with the ion is gradually replaced by carbonyl oxygen atoms at the entrance of the channel; after completely entering the channel ($|z|<$9 Å), only two single-file water molecules located before and after the ion in the channel can form coordination with the ion, and the carbonyl oxygen atoms of different residues in gA can contribute ∼4 additional coordination numbers with the ion.

After the ion enters the channel, the carbonyl oxygen atoms that form coordination with the ion are continuously replaced. FIG. 5 shows the distance distribution of the ion from carbonyl oxygen atoms at different positions as the ion passes through a series of binding sites in the channel. It can be seen that there are always four carbonyl oxygen atoms forming coordination with the ion, and during permeation, two carbonyl oxygen atoms at the same binding site are gradually replaced by two carbonyl oxygen atoms at the next binding site, thus maintaining the hydration state of the ion. The continuous replacement of coordinated carbonyl oxygen atoms is also manifested in the fluctuation of the diffusion coefficients (FIG. 3) and the distribution of extreme points of the free energy profile (FIG. 2). These results are in excellent agreement with our previous work [31].

When comparing the coordination number and coordination atom rearrangement data (FIG. 4 and FIG. 5), it can be found that, for single- and double-channel systems, there is almost no difference in the coordination of ion with single-file water and gA carbonyl oxygen atoms after the ion enters the channel. This indicates that the higher conductance of the double-channel does not come from the direct contribution of single-file water or carbonyl oxygen atoms in the channel.

On the other hand, as shown in FIG. 4, for the double-channel system, before the ion fully enters the channel ($|z|>$ 9 Å), both K^+ and Na^+ possess slightly lower coordination numbers of water outside the channel than that for the single-channel system, suggesting that water outside the channel may have a greater contribution to the higher conductance of the double-channel.

D. Free energy contributions during the K^+/Na^+ permeation

To quantify the contribution of different components in the system to the ion passing through the gA channel, we further decomposed the free energy change into the

DOI:10.1063/1674-0068/cjcp2103046

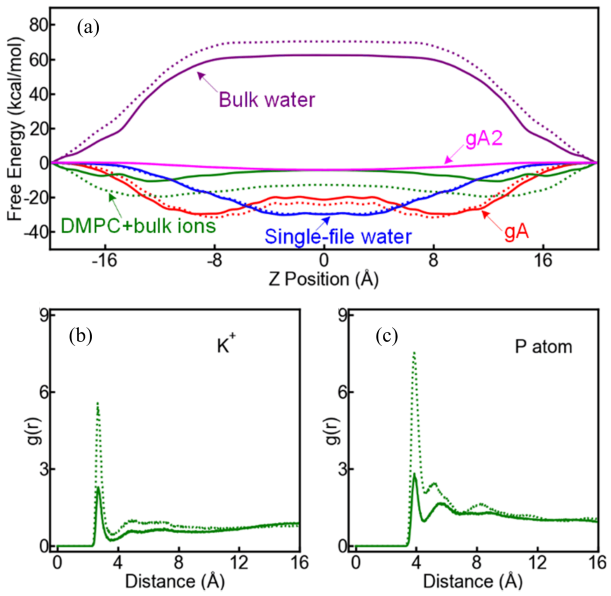

FIG. 6 (a) Free energy decomposition of K^+. The RDF of (b) bulk cation and (c) phosphate group within DMPC when ion passing through single- and double-gA channels. The dashed and solid lines refer to the data in single- and double-channel systems, respectively.

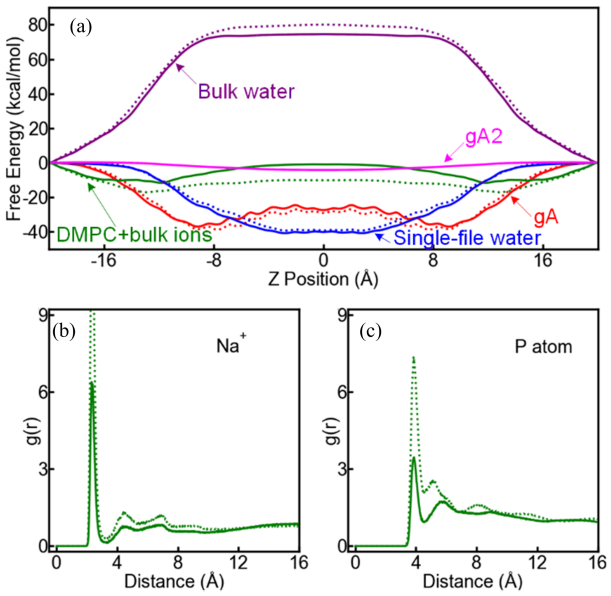

FIG. 7 (a) Free energy decomposition of Na^+. The RDF of (b) bulk cation or (c) phosphate group within DMPC when ion passing through single- and double-gA channels. The dashed and solid lines refer to the data in single- and double-channel systems, respectively.

contributions of DMPC+bulk ions, bulk water, single-file water in the channel, and the gA channel itself (and the second gA channel). As shown by the dashed lines in FIG. 6(a) and 7(a), the process of K^+ or Na^+ passing through the single-channel can be described by the following steps:

(i) Ion entry into the channel: This process is mainly driven by the attraction of DMPC and gA protein to the ion. It can be seen from FIG. 2 that the total free energy profile has deep wells on both the outer and inner sides of the channel entrance. The free energy decomposition in FIG. 6(a) and FIG. 7(a) further show that the ion-binding sites on the outer and inner sides of the channel are located near $|z|$=12 Å and $|z|$=9 Å, respectively. The electrostatic interaction of the DMPC headgroup attracts the ion to the outside of the channel, after which the attraction of the gA protein guides the ion to the inner binding sites of the channel.

(ii) Ion migration in the channel: After the ion enters the channel, it is completely isolated from the bulk water, and the free energy contribution of the bulk water reaches a plateau phase. At this time, the movement of the ion is mainly driven by the gA protein and the single-file water in the channel. At the center of the channel, the contribution of single-file water is even stronger than that of the gA protein. Since the free energy contributions of DMPC, single-file water, and gA protein are opposite to the contributions of bulk water, the contributions of these components can be regarded as energy compensation for the ion dehydration.

(iii) Ion exit from the channel: This process is the reverse of the ion entry process, in which the ion moves from the inner binding site of the channel to the outer binding site of the channel and then dissolves again in the bulk water.

The free energy decomposition data of ions passing through the channel in this work are similar to those previously reported [25, 31]. When comparing the contributions of different components to the free energy, it is clear that for the single- and double-channel systems, the energy difference of the single-file water as well as the gA protein is very small, which is consistent with the results of the coordination numbers above. This data further shows that the high conductance of the double-channel does not originate from the contribution of the single-file water or the gA protein. For the double-channel system, the other gA protein (gA2, the solid magenta line in FIG. 6(a) and FIG. 7 (a)) contributes almost zero free energy to the ion in the first channel, indicating that when two gAs dimerize to form a double-channel, the presence of the second channel does not directly affect the movement of ions in the

DOI:10.1063/1674-0068/cjcp2103046

first channel.

However, the presence of the second channel directly affects the distribution of cations, negatively charged phosphate groups in the DMPC head group, and bulk water at the entrance of the first channel. As shown in FIG. 6(b, c) and FIG. 7(b, c), distributions of the phosphate group and the bulk cation at the channel entrance are lower in the double-channel system than in the single-channel system, and the distribution of phosphate group changes more than that of the cation. This causes a weakening of the attraction of the DMPC and the bulk ion, thereby reducing the free energy contribution of both (the solid green line in FIG. 6(a)). Besides, the presence of a second channel also affects the distribution of bulk water at the channel entrance, resulting in a slightly lower coordination number for ions with the bulk water in the double-channel system than in the single-channel system (the solid blue line in FIG. 4). It makes the contribution of the bulk water slightly weaker in the double-channel system than in the single-channel system.

In the double-channel system, the contributions of DMPC and bulk ions and bulk water to the free energy are weakened, but the magnitude of the free energy change is greater for DMPC and bulk ions, which reduces the binding affinity of ions to the channel (FIG. 2) and accelerates the diffusion of ions in the channel (FIG. 3), resulting in a higher conductance of double-channel gA. This result is consistent with the findings reported by Kuyucak *et al.* [51] that phospholipid head groups and bulk water outside the channel have a greater effect on the conductance of gA channels in different membrane environments, suggesting that gA dimerization affects the cation-transport properties by adjusting the environment around the gA protein rather than directly adjusting the conformation of the gA protein.

IV. CONCLUSION

In summary, we performed umbrella sampling MD simulations with AMOEBA polarizable force field to study the mechanism of dimerization which affect the ion-transport properties of gA channels. The calculated conductance of K^+ and Na^+ passing through the channels are in excellent agreement with the experimental data. In the double-channel system, the second channel affects the distribution of bulk ions, phospholipid headgroups, and bulk water at the entrance of the first channel, rendering the double-channel gA a higher conductance. This result indicates that the effect of gA dimerization on ion passing through the channel is achieved by adjusting the environment around the gA protein and also shows that the AMOEBA polarizable force field has high reliability in ion channel simulations.

It should be noted that only the simulation results of single- and double-channel gAs in DMPC phospholipid bilayers were compared in this work. In real cellular environment, the composition of the membrane is extremely complex, and the aggregated form of ion channels is not limited to the two-channel structure. Therefore, simulations with three-channel, four-channel, or even more complex channel structures are required in subsequent studies, and different types of phospholipid molecules are also needed to systematically explore the regulation mechanisms of protein aggregation on ion channel function.

V. ACKNOWLEDGMENTS

This work is supported by the National Natural Science Foundation of China (No.21933010).

[1] C. Maffeo, S. Bhattacharya, J. Yoo, D. Wells, and A. Aksimentiev, Chem. Rev. **112**, 6250 (2012).
[2] M. Chavent, A. L. Duncan, and M. S. P. Sansom, Curr. Opin. Struct. Biol. **40**, 8 (2016).
[3] Y. L. Zhao, P. M. U. Ung, G. Zohoranszky-Kohalmi, A. V. Zakharov, N. J. Martinez, A. Simeonov, I. W. Glaaser, G. Rai, A. Schlessinger, J. J. Marugan, and P. A. Slesinger, Cell Rep. **31**, 17 (2020).
[4] I. Casuso, J. Khao, M. Chami, P. Paul-Gilloteaux, M. Husain, J. P. Duneau, H. Stahlberg, J. N. Sturgis, and S. Scheuring, Nat. Nanotechnol. **7**, 525 (2012).
[5] M. Chavent, A. L. Duncan, P. Rassam, O. Birkholz, J. Helie, T. Reddy, D. Beliaev, B. Hambly, J. Piehler, C. Kleanthous, and M. S. P. Sansom, Nat. Commun. **9**, 2846 (2018).
[6] A. D. Dupuy and D. M. Engelman, Proc. Natl. Acad. Sci. USA **105**, 2848 (2008).
[7] M. L. Molina, A. M. Giudici, J. A. Poveda, G. Fernandez-Ballester, E. Montoya, M. L. Renart, A. M. Fernandez, J. A. Encinar, G. Riquelme, A. Morales, and J. M. Gonzalez-Ros, J. Biol. Chem. **290**, 25745 (2015).
[8] M. A. Principalli, L. Lemel, A. Rongier, A. C. Godet, K. Langer, J. Revilloud, L. Darre, C. Domene, M. Vivaudou, and C. J. Moreau, Biochim. Biophys. Acta Biomembr. **1859**, 2144 (2017).
[9] A. Sumino, D. Yamamoto, M. Iwamoto, T. Dewa, and S. Oiki, J. Phys. Chem. Lett. **5**, 578 (2014).

DOI:10.1063/1674-0068/cjcp2103046

[10] A. L. Duncan, T. Reddy, H. Koldso, J. Helie, P. W. Fowler, M. Chavent, and M. S. P. Sansom, Sci. Rep. **7**, 16647 (2017).
[11] K. M. Visscher, J. Medeiros-Silva, D. Mance, J. Rodrigues, M. Daniels, A. Bonvin, M. Baldus, and M. Weingarth, Angew. Chem. Int. Ed. Engl. **56**, 13222 (2017).
[12] T. A. Harroun, W. T. Heller, T. M. Weiss, L. Yang, and H. W. Huang, Biophys. J. **76**, 937 (1999).
[13] R. L. Goforth, A. K. Chi, D. V. Greathouse, L. L. Providence, R. E. Koeppe, and O. S. Andersen, J. Gen. Physiol. **121**, 477 (2003).
[14] L. Al-Momani, P. Reiss, and U. Koert, Biochem. Biophys. Res. Commun. **328**, 342 (2005).
[15] D. K. Chistyulin, T. I. Rokitskaya, S. I. Kovalchuk, A. I. Sorochkina, A. M. Firsov, E. A. Kotova, and Y. N. Antonenko, Biochim. Biophys. Acta Biomembr. **1859**, 896 (2017).
[16] J. Yoo and Q. Cui, Biophys. J. **104**, 128 (2013).
[17] Y. P. Yang, L. P. He, J. X. Bao, Y. F. Qi, and J. Z. H. Zhang, Chin. J. Chem. Phys. **32**, 134 (2019).
[18] Z. S. Yu, Y. Y. Gao, X. G. Wang, G. Q. Zhou, S. W. Zeng, and J. L. Chen, Chin. J. Chem. Phys. **31**, 85 (2018).
[19] Y. Huang, H. C. Xu, and J. L. Liao, Chin. J. Chem. Phys. **33**, 712 (2020).
[20] W. C. Lin, S. P. Tan, S. F. Zhou, X. J. Zheng, W. J. Wu, and K. C. Zheng, Chin. J. Chem. Phys. **30**, 429 (2017).
[21] C. Tian, K. Kasavajhala, K. A. A. Belfon, L. Raguette, H. Huang, A. N. Migues, J. Bickel, Y. Wang, J. Pincay, Q. Wu, and C. Simmerling, J. Chem. Theory Comput. **16**, 528 (2020).
[22] R. B. Best, X. Zhu, J. Shim, P. E. M. Lopes, J. Mittal, M. Feig, and A. D. MacKerell, J. Chem. Theory Comput. **8**, 3257 (2012).
[23] B. Roux and M. Karplus, Biophys. J. **59**, 961 (1991).
[24] G. A. Olah, H. W. Huang, W. H. Liu, and Y. L. Wu, J. Mol. Biol. **218**, 847 (1991).
[25] T. W. Allen, O. S. Andersen, and B. Roux, Proc. Natl. Acad. Sci. USA **101**, 117 (2004).
[26] H. I. Ingolfsson, Y. H. Li, V. V. Vostrikov, H. Gu, J. F. Hinton, R. E. Koeppe, B. Roux, and O. S. Andersen, J. Phys. Chem. B **115**, 7417 (2011).
[27] T. Giorgino and G. De Fabritiis, J. Chem. Theory Comput. **7**, 1943 (2011).
[28] H. D. Song and T. L. Beck, J. Phys. Chem. C **117**, 3701 (2013).
[29] T. W. Allen, O. S. Andersen, and B. Roux, Biophys. J. **90**, 3447 (2006).
[30] H. Chu, X. Peng, Y. Li, Y. Zhang, and G. Li, Molecules **23**, 77 (2017).
[31] X. Peng, Y. Zhang, H. Chu, Y. Li, D. Zhang, L. Cao, and G. Li, J. Chem. Theory Comput. **12**, 2973 (2016).
[32] B. G. Pierce, Y. Hourai, and Z. P. Weng, Plos One **6**, e24657 (2011).
[33] P. Eastman, J. Swails, J. D. Chodera, R. T. McGibbon, Y. Zhao, K. A. Beauchamp, L. P. Wang, A. C. Simmonett, M. P. Harrigan, C. D. Stern, R. P. Wiewiora, B. R. Brooks, and V. S. Pande, PLoS Comput. Biol. **13**, e1005659 (2017).
[34] J. A. Rackers, Z. Wang, C. Lu, M. L. Laury, L. Lagardere, M. J. Schnieders, J. P. Piquemal, P. Y. Ren, and J. W. Ponder, J. Chem. Theory Comput. **14**, 5273 (2018).
[35] U. Essmann, L. Perera, M. L. Berkowitz, T. Darden, H. Lee, and L. G. Pedersen, J. Chem. Phys. **103**, 8577 (1995).
[36] J. J. Goings, F. Ding, and X. Li, S*elf-Consistent Field using Direct Inversion in Iterative Subspace Method and Quasi-Newton Vectors. In Proceedings of Mest 2012: Electronic Structure Methods with Applications to Experimental Chemistry*, P. E. Hoggan Ed., San Diego: Elsevier Academic Press Inc., Vol. 68, 77 (2014).
[37] A. H. Wang, Z. C. Zhang, and G. H. Li, Chin. J. Chem. Phys. **32**, 277 (2019).
[38] G. A. Tribello, M. Bonomi, D. Branduardi, C. Camilloni, and G. Bussi, Comput. Phys. Commun. **185**, 604 (2014).
[39] J. S. Hub, B. L. de Groot, and D. van der Spoel, J. Chem. Theory Comput. **6**, 3713 (2010).
[40] M. J. Abraham, T. Murtola, R. Schulz, S. Páll, J. C. Smith, B. Hess, and E. Lindahl, SoftwareX **1-2**, 19 (2015).
[41] H. L. Tepper and G. A. Voth, J. Phys. Chem. B **110**, 21327 (2006).
[42] S. J. Marrink and H. J. C. Berendsen, J. Phys. Chem. **98**, 4155 (1994).
[43] S. W. I. Siu and R. A. Bockmann, J. Phys. Chem. B **113**, 3195 (2009).
[44] T. Bastug, S. M. Patra, and S. Kuyucak, Chem. Phys. Lipids **141**, 197 (2006).
[45] M. Kato and A. Warshel, J. Phys. Chem. B **109**, 19516 (2005).
[46] J. E. Straub, M. Borkovec, and B. J. Berne, J. Phys. Chem. **91**, 4995 (1987).
[47] S. Crouzy, T. B. Woolf, and B. Roux, Biophys. J. **67**, 1370 (1994).
[48] D. G. Levitt, Annu. Rev. Biophys. Biophys. Chem. **15**, 29 (1986).
[49] T. W. Allen, O. S. Andersen, and B. Roux, Biophys. Chem. **124**, 251 (2006).
[50] B. Roux, T. Allen, S. Berneche, and W. Im, Q. Rev. Biophys. **37**, 15 (2004).
[51] J. Setiadi and S. Kuyucak, Membranes **6**, 20 (2016).

DOI:10.1063/1674-0068/cjcp2103046